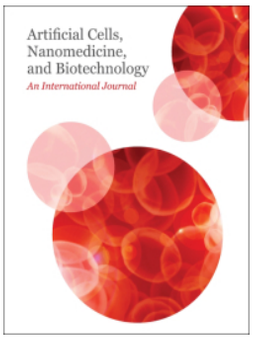

Taylor & Francis
Taylor & Francis Group

Artificial Cells, Nanomedicine, and Biotechnology
An International Journal

ISSN: 2169-1401 (Print) 2169-141X (Online) Journal homepage: www.tandfonline.com/journals/ianb20

Advancing bone tissue engineering: anisotropic performance of poly(lactic-co-glycolic acid) (PLGA) composites with nano-calcium sulphate (nCS) and fucoidan (fu)

Norshazliza Ab Ghani, Mohammed Rafiq Abdul Kadir, Sathiya Maran, Izdihar Kamal, Muhammad Khalis Abdul Karim, Mohd Hafiz Mohd Zaid, Hanumanth Rao Balaji Raghavendran, Muhammad Hanif Ramlee, Tunku Kamarul Zaman & Muhammad Imam Ammarullah

To cite this article: Norshazliza Ab Ghani, Mohammed Rafiq Abdul Kadir, Sathiya Maran, Izdihar Kamal, Muhammad Khalis Abdul Karim, Mohd Hafiz Mohd Zaid, Hanumanth Rao Balaji Raghavendran, Muhammad Hanif Ramlee, Tunku Kamarul Zaman & Muhammad Imam Ammarullah (2026) Advancing bone tissue engineering: anisotropic performance of poly(lactic-co-glycolic acid) (PLGA) composites with nano-calcium sulphate (nCS) and fucoidan (fu), Artificial Cells, Nanomedicine, and Biotechnology, 54:1, 53-73, DOI: 10.1080/21691401.2025.2582447

To link to this article: https://doi.org/10.1080/21691401.2025.2582447

Published online: 02 Jan 2026.

ARTIFICIAL CELLS, NANOMEDICINE, AND BIOTECHNOLOGY
2026, VOL. 54, NO. 1, 53–73
https://doi.org/10.1080/21691401.2025.2582447

Taylor & Francis
Taylor & Francis Group

Advancing bone tissue engineering: anisotropic performance of poly(lactic-co-glycolic acid) (PLGA) composites with nano-calcium sulphate (nCS) and fucoidan (fu)

Norshazliza Ab Ghani[a], Mohammed Rafiq Abdul Kadir[b], Sathiya Maran[c], Izdihar Kamal[d], Muhammad Khalis Abdul Karim[d], Mohd Hafiz Mohd Zaid[d], Hanumanth Rao Balaji Raghavendran[a,e], Muhammad Hanif Ramlee[f,g], Tunku Kamarul Zaman[a] and Muhammad Imam Ammarullah[f,h,i]

[a]Tissue Engineering Group, National Orthopaedic Centre of Excellence for Research and Learning (NOCERAL), Faculty of Medicine, Universiti Malaya, Kuala Lumpur, Malaysia; [b]Department of Biomedical Engineering, Faculty of Engineering, Universiti Malaya, Kuala Lumpur, Malaysia; [c]School of Pharmacy, Monash University Malaysia, Subang Jaya, Malaysia; [d]Department of Physics, Faculty of Science, University Putra Malaysia, Serdang, Malaysia; [e]Biomaterials Laboratory, Faculty of Clinical Research, Central Research Facility, Sri Ramachandra Institute of Higher Education and Research, Chennai, India; [f]Bone Biomechanics Laboratory (BBL), Department of Biomedical Engineering and Health Sciences, Faculty of Electrical Engineering, Universiti Teknologi Malaysia, Johor Bahru, Malaysia; [g]Rehabilitation Nexus (RehabNex) Research Group, Health and Wellness Research Alliance, Universiti Teknologi Malaysia, Johor Bahru, Malaysia; [h]Undip Biomechanics Engineering & Research Centre (UBM-ERC), Universitas Diponegoro, Monrovia, Semarang, Liberia; [i]Department of Mechanical Engineering, Faculty of Engineering, Universitas Diponegoro, Semarang, Indonesia

ABSTRACT

This study investigates the anisotropic properties of three different poly(lactic-co-glycolic acid) (PLGA)-based materials: PLGA with nano-calcium sulphate (nCS), PLGA with fucoidan (fu) and PLGA with both nCS and fu. Using finite element analysis (FEA), the study explores their potential applications in bone tissue engineering. Anisotropy, or the directional dependency of mechanical properties, is critical in designing biomaterials for bone regeneration due to the complex, hierarchical structure of natural bone. The objective was to evaluate the mechanical behaviour of each composite material under simulated physiological conditions, focusing on their anisotropic responses to loading. The findings indicate that PLGA-nCS exhibited the highest degree of anisotropy, with enhanced stiffness and strength along preferred load-bearing directions, making it suitable for applications requiring higher mechanical stability. In contrast, PLGA-nCS-fu demonstrated moderate mechanical strength but displayed isotropic behaviour, ensuring consistent compressive performance across all directions. The study highlights the synergistic effects of incorporating nCS and fu into PLGA-based materials. fu, a natural sulphated polysaccharide derived from brown seaweed, significantly enhances the biological performance of these composites.

ARTICLE HISTORY
Received 8 August 2025
Revised 12 October 2025
Accepted 27 October 2025

KEYWORDS
Poly(lactic-co-glycolic acid) (PLGA); nano-calcium sulphate (nCS); fucoidan (fu); finite element model (FEM); bone tissue engineering

Introduction

Bone tissue engineering represents a critical frontier in regenerative medicine, aiming to develop biomaterials capable of supporting, repairing or regenerating damaged bone [1]. Central to this endeavour is the challenge of mimicking the complex structural and mechanical characteristics of native bone tissue. Among these characteristics, anisotropy, which is the variation of mechanical properties based on the direction of applied force that plays a pivotal role [2,3]. Bone's anisotropic behaviour stems from its hierarchical organization, comprising a multi-scale structure that endows it with both stiffness and resilience. This structural anisotropy enables bone to endure diverse physiological loads while maintaining integrity and function [3].

CONTACT Mohammed Rafiq Abdul Kadir rafiqkadir@um.edu.my Department of Biomedical Engineering, Faculty of Engineering, Universiti Malaya, Kuala Lumpur 50603, Federal Territory of Kuala Lumpur, Malaysia; Muhammad Imam Ammarullah imamammarullah@gmail.com Department of Mechanical Engineering, Faculty of Engineering, Universitas Diponegoro, Semarang 50275, Central Java, Indonesia

Reproducing this anisotropic nature in synthetic scaffolds remains a significant challenge in the design of biomaterials for bone regeneration. Bone's directional mechanical performance is essential for its load-bearing capability and resistance to deformation or failure under stress [4]. Consequently, any material intended to replace or support bone must not only be biocompatible but must also exhibit directional strength and stiffness to integrate functionally with the host tissue [5,6]. This requirement shows the need for advanced biomaterials that go beyond isotropic mechanical responses to more closely mimic the physiological behaviour of bone.

Poly(lactic-co-glycolic acid) (PLGA) has emerged as a widely studied polymer in bone tissue engineering due to its favourable characteristics, including biocompatibility, controlled biodegradability and adaptable mechanical properties [7]. However, pure PLGA typically exhibits isotropic mechanical behaviour, limiting its effectiveness in applications where anisotropic responses are crucial [8]. This mechanical limitation has prompted researchers to investigate composite formulations by incorporating bioactive fillers or modifiers that can impart anisotropic features while enhancing overall scaffold functionality.

Among the promising candidates for composite design are nano-calcium Sulphate (nCS) and fucoidan (fu), each offering distinct advantages. nCS is known to significantly enhance the compressive strength and osteoconductivity of PLGA, contributing to better mechanical integration with native bone [9,10]. fu, a sulphated polysaccharide derived from brown seaweed, offers a spectrum of biological functions, including anti-inflammatory, antioxidant and osteogenic activities, making it a valuable additive for promoting cellular behaviour essential for bone repair [11]. When combined with PLGA, these additives offer the potential to develop multifunctional scaffolds that are not only mechanically robust but also biologically responsive.

This study utilizes finite element analysis (FEA), a computational simulation technique, to evaluate the anisotropic mechanical behaviour of three PLGA-based composites: PLGA-nCS, PLGA-fu and PLGA-nCS-fu. FEA enables detailed modelling of mechanical responses under physiological loading conditions, making it a powerful tool for assessing the directional performance of biomaterials [12]. Through simulating the mechanical environment of bone, FEA allows for an in-depth comparison of how different composite configurations respond to stress along various axes, offering insights into their suitability for load-bearing applications [13].

Ultimately, this research aims to identify which composite formulation best replicates the anisotropic mechanical behaviour of natural bone while maintaining the necessary biological functionality. The findings are expected to inform the design and selection of next-generation scaffolds in bone tissue engineering, particularly those requiring both structural support and enhanced biological interaction. With integrating nCS and fu into PLGA-based scaffolds and analysing their anisotropic characteristics, this study contributes to the development of advanced biomaterials that more closely match the physiological and functional demands of bone tissue, thereby improving the efficacy of regenerative therapies.

Method

This study employed a combination of Mimics Materialize and ANSYS software to perform FEA on three different materials as explained in Figure 1: for each of the materials – (A) PLGA-nCS-fu, (B) PLGA-nCS and (C) PLGA-fu; the mechanical responses were evaluated by analysing seven different samples. Each sample was tested for its ability to withstand compressive stresses while monitoring the displacement, deformation and stress distribution across the material.

microCT analysis

The microstructural of the scaffolds was analysed using high-resolution micro-computed tomography (CT) (microCT, Bruker Skyscan 1172). Each scaffold was scanned at a voxel resolution of 9 µm with an X-ray source set at 80 kV and 100 µA [14] and a 0.5 mm aluminium filter was applied to minimize beam hardening artefacts. Samples were mounted on a 360° rotating stage, with projection images captured at 0.4° rotation steps and frame averaging of 2 to enhance image quality. Calibration was performed using standard density phantoms (aluminium and polystyrene) to ensure greyscale accuracy. The raw data were reconstructed using NRecon software (version 1.6.10.4) with beam hardening correction, ring artefact suppression, and Gaussian smoothing applied. Post-reconstruction image analysis was conducted using CTAn and mimics software to evaluate internal architecture, pore size distribution and total porosity. All images were threshold based on standard histogram values to differentiate scaffold material from background noise.

3D model creation using Mimics Materialize

Mimics Materialize software was utilized to create detailed 3D models of bone scaffold structures for each PLGA-based material. Mimics Materialize facilitates the

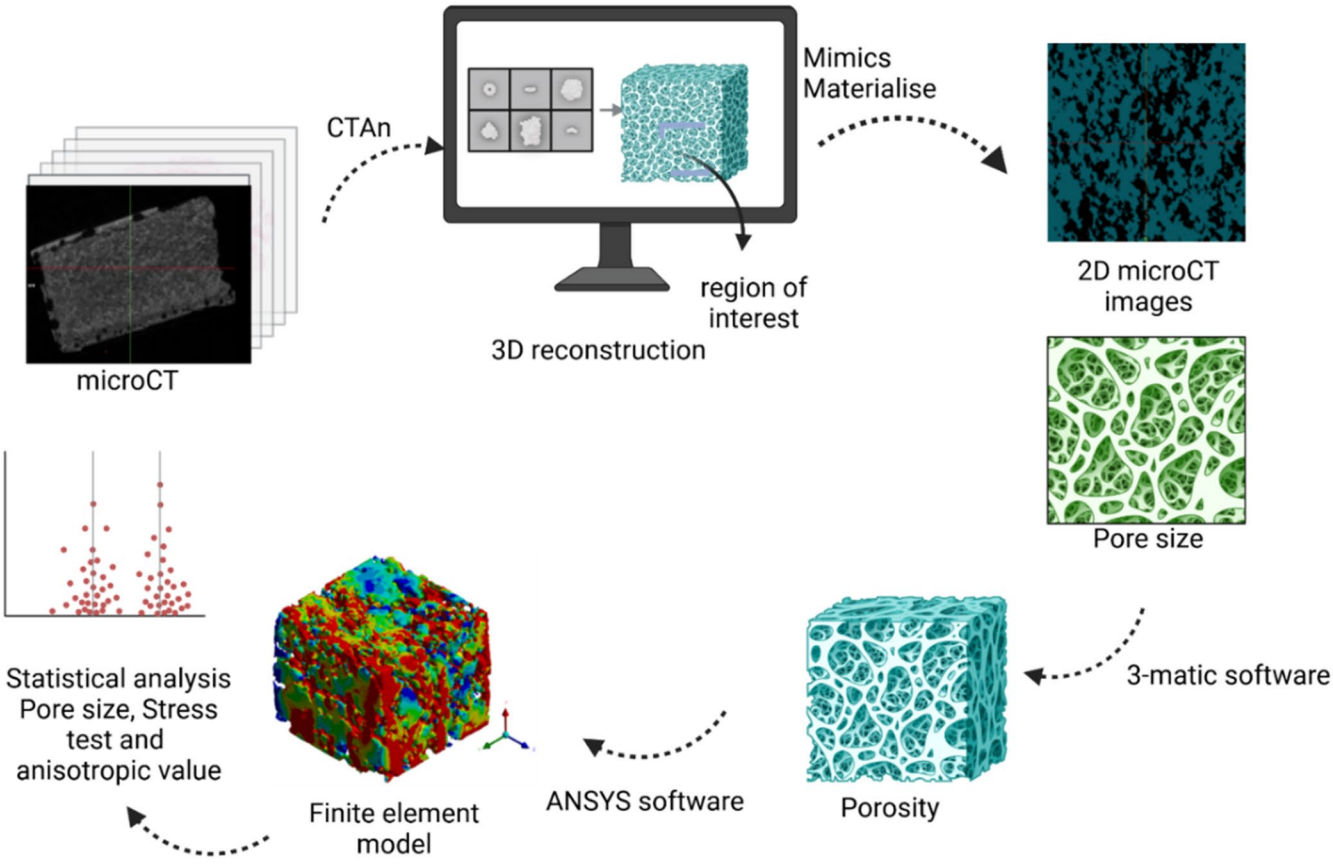

Figure 1. A comparative analysis of three different polymer-ceramic composite-each cube represents a virtual model of porous PLGA-based composite. The differences colours indicate varying levels of mechanical stress or strain under a simulated load (the vertical arrows suggest the direction of the applied force).

generation of high-resolution models based on CT data. In this study, material designs for each scaffold were generated to replicate the structural properties essential for bone tissue engineering. These models were subsequently refined to accurately represent the anisotropic features of each material. All images were threshold based on standard histogram values to differentiate scaffold material from background noise.

Pore size analysis

To accurately determine the pore size distribution, a systematic approach was employed using Mimics Materialize software. First, a threshold was established to distinguish the target regions, followed by the construction of a 3D dataset from 500 CT slices. The greyscale values were set to 100% volume, ensuring optimal visualization of the porous structures. Key anatomical regions, including the anterior, posterior, top and bottom, were identified to maintain consistency in segmentation.

The thresholding technique was applied to segment the structure, with Hounsfield units ranging from 35 to 255 used to select the material itself, while HU values below 35 were classified as pores. Due to data size constraints, a cropped mask (500 mm × 500 mm × 500 mm) was extracted and saved for further analysis, as generating a 3D model for the entire sample was computationally intensive. The segmented 3D data were then exported as an STL file, enabling further geometric assessment.

For pore size quantification, the pore size ruler tool in Mimics Materialize was utilized to measure 200 pore diameters per sample, ensuring statistical robustness. Given that each experimental group consisted of seven samples, a total of 1400 pore size readings were recorded. This high-resolution measurement approach provided a comprehensive pore size distribution analysis, enhancing the accuracy and reproducibility of the results. Through standardizing this method, the study ensures precision in evaluating scaffold porosity, a critical factor in optimizing nutrient transport and cell infiltration for tissue engineering applications.

Porosity

To analyse the porosity of the scaffold, 3-Matic and Mimics Materialize software were employed for a detailed 3D reconstruction and FEA. Initially, thresholding parameters were adjusted, setting the minimum

value to 0 and the maximum value at the middle intensity range, ensuring accurate segmentation of the porous structure. A mask shift was applied, differentiating regions with green and yellow indicators to enhance visualization. The 3D construction of the porous structure was then performed, allowing a comprehensive assessment of scaffold architecture.

Subsequently, the segmented model was processed in 3-Matic, where the STL file was imported, and a 3D model was generated. To ensure mesh quality, remeshing was performed using uniform remesh settings, followed by the application of tetrahedral (Tet-4) volume meshing to create a finite element-ready model. Upon successful meshing, the model was saved and exported for further analysis in ANSYS, enabling a detailed evaluation of the scaffold's mechanical behaviour under simulated physiological conditions. This standardized approach ensures high precision in porosity quantification, allowing for an accurate assessment of scaffold performance in terms of mechanical stability, nutrient diffusion and cell infiltration, which are critical for tissue engineering applications.

Finite element model development

To evaluate the mechanical behaviour of the scaffold structure, a FEA was conducted using ANSYS Workbench. The external model was first imported by selecting the required. cdb external file, followed by an update in the setup panel to ensure proper integration of the dataset. A static structural analysis system was initialized, and the engineering data module was used to define the material properties of PLGA-nCS-fu, with an assigned Young's modulus of 12 GPa and a Poisson's ratio of 0.3. The total number of elements for all 21 models ranged from 850,000 to 1,000,000 tetrahedral elements. To apply the loading conditions, named selections were used to define the top layer of the scaffold, and nodal displacement was assigned to simulate a 1% compression of the sample, ensuring a controlled deformation analysis. A fixed support was applied to constrain the model, preventing unintended motion during simulation (Figure 2).

The porosity percentage (mean) of three different biomaterial composites used for bone tissue engineering applications, there are PLGA-nCS-fu, PLGA-nCS and PLGA-fu was shown in Figure 3. The y-axis represents the porosity percentage, while the x-axis lists the different samples. Error bars are included to indicate the variability or standard deviation in the measurements. Porosity is a key factor that affects the biological performance and mechanical properties of scaffolds used in bone regeneration, influencing cell infiltration, nutrient diffusion, and mechanical strength. The assessments were performed using one-way ANOVA and post-hoc test and were statistically significant if $*p < 0.05$; p value = 0.000482342.

The results were retrieved by inserting total deformation and equivalent von Mises stress under the solution module, enabling a detailed assessment of the scaffold's structural response under the applied compression. The von Mises stress distribution was

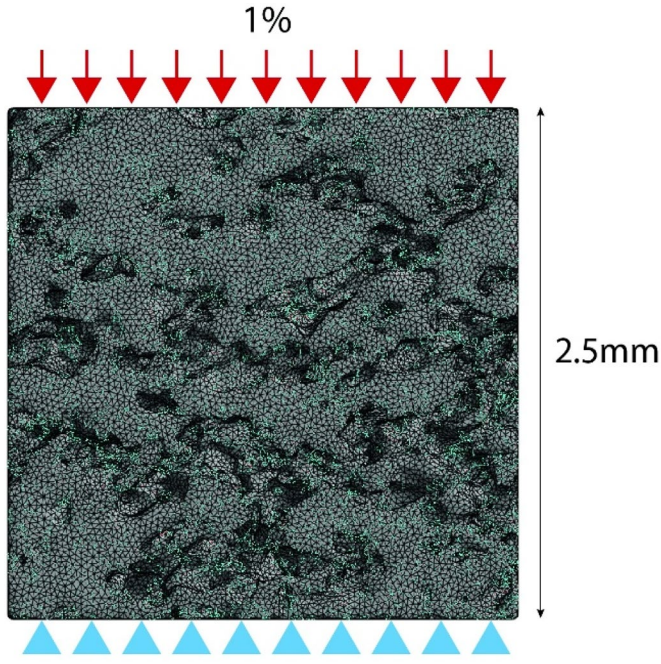

Figure 2. Finite element model of simulated bone scaffold.

analysed, providing insights into stress concentration zones within the porous structure. The wireframe display was removed to enhance visualization, ensuring a clear interpretation of deformation and stress patterns.

To analyses the anisotropic behaviour of the model, two additional simulations were performed with the same 1% compressive nodal displacement but applied along the other two axes (Y-axis and Z-axis). Since each model underwent analysis along three axes, a total of 63 FEA simulations were conducted. The ANSYS Workbench project was saved to ensure reproducibility and facilitate further optimization of the scaffold design. This approach provides a comprehensive finite element-based mechanical evaluation, ensuring that the scaffold meets the required structural integrity for tissue engineering applications while maintaining optimal pore interconnectivity for cell infiltration and nutrient transport.

Data interpretation

Following the simulations, the data were analysed to compare the mechanical performance of each composite in terms of anisotropy, strength and stiffness. To determine the effective stiffness of the scaffold, numerical results from ANSYS Workbench were processed using excel for statistical analysis. The median value of the dataset was extracted using the MEDIAN (B2:B200000) function, ensuring a robust measure of central tendency while minimizing the influence of extreme values. A histogram analysis was performed to visualize the distribution of stiffness values, and all zero values were removed to enhance data accuracy. The median stiffness value was then normalized by dividing it by the applied strain, considering that the model was loaded with a 1% nodal displacement. The effective stiffness was therefore calculated as 68 MPa divided by 1% strain, yielding a stiffness value of 6.8 GPa. This method provides a quantitative assessment of scaffold rigidity, allowing for precise evaluation of mechanical stability and structural performance in relation to porosity variations.

Statistical analysis

Statistical analysis was conducted using OriginPro version 2024. Prior to one-way analysis of variance (ANOVA), data normality was assessed using the Shapiro–Wilk test, and homogeneity of variance was tested using Levene test ($p > 0.05$). All 21 groups showed p values > 0.05 in the Shapiro–Wilk test, indicating no significant deviation from normality. One-way ANOVA was then performed to access group differences, followed by Tukey's *post hoc* test for pairwise comparison. A p value of <0.05 was considered statistically significant.

Results

Microstructure of materials

PLGA and nCS composites are widely used in bone tissue engineering due to their biocompatibility and degradation properties [9,15]. The microCT images reveal a specific microstructural pattern characterized by a uniform pore distribution. However, the grey value histograms highlight some variability in porosity (Table 1) across different samples, particularly in pore size distribution. The histograms associated with each sample show a range of grey intensities, correlating with the density distribution of the materials. The microstructures of the samples display small, well-distributed pores, indicative of homogeneous structural formation. However, slight variations in grey value peaks suggest differences in density within certain areas of the samples, likely caused by inconsistencies in the mixing process or nCS particle agglomeration.

Porosity plays a crucial role in determining the biological performance and mechanical properties of scaffolds for bone regeneration, impacting cell infiltration, nutrient diffusion and structural integrity. The data were analysed using one-way ANOVA followed by Tukey's *post hoc* test, with statistical significance set at $p < 0.05$. As shown in Figure 4, a significant difference in mean pore size was observed among the scaffold groups ($p = 0.00048$). To ensure robust analysis, 200 pore size measurements were recorded for each sample, resulting in a total of 1400 data points per material group ($n = 7$). These measurements provided a comprehensive assessment of the pore size distribution across the PLGA-nCS-fu, PLGA-nCS and PLGA-Fu scaffolds.

The incorporation of fu introduces significant changes to the microstructure of PLGA-nCS-fu composites. MicroCT images show that fu enhances the uniformity of pore distribution, likely due to its influence on the polymer network and its interactions with PLGA and nCS particles [16]. The grey value histograms for PLGA-nCS-fu samples exhibit a broader range of values, suggesting a wider variety of pore sizes and density distributions compared to PLGA-nCS materials. fu appears to act as a stabilizer, preventing nCS particle agglomeration and contributing to a more evenly distributed microstructure [17]. Notably, the histograms for fu-incorporated materials show more prominent peaks at lower grey values, indicating the presence of more porous or lower-density regions.

The PLGA-nCS-fu materials exhibit a more homogeneous microstructure compared to PLGA-nCS materials. The histograms for PLGA-nCS materials display multiple peaks or irregular distributions, whereas the fu-containing samples show more streamlined, single

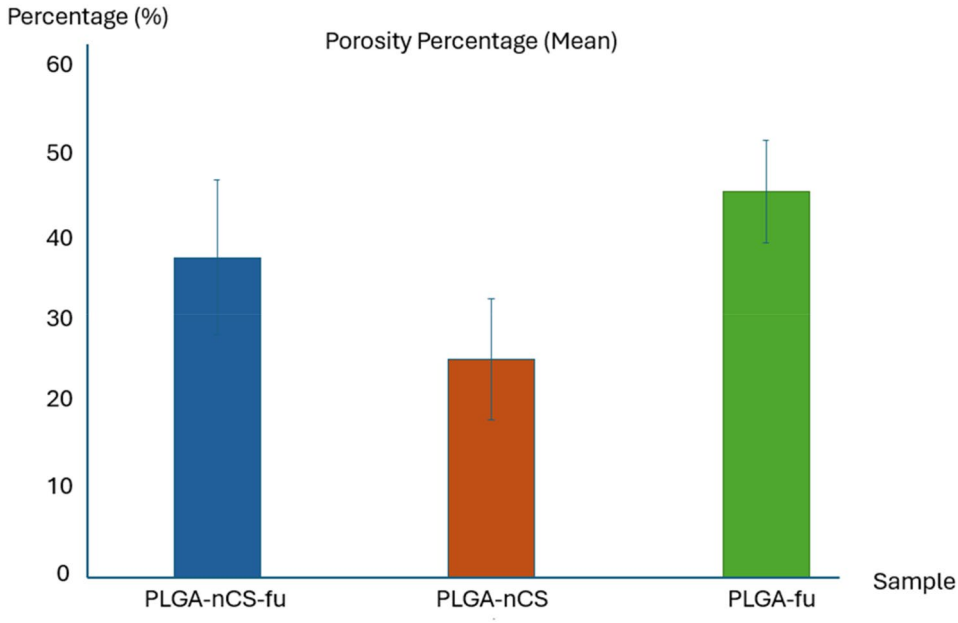

Figure 3. The porosity percentage (mean) of three different biomaterial composites used for bone tissue engineering applications: PLGA-nCS-fu, PLGA-nCS and PLGA-fu.

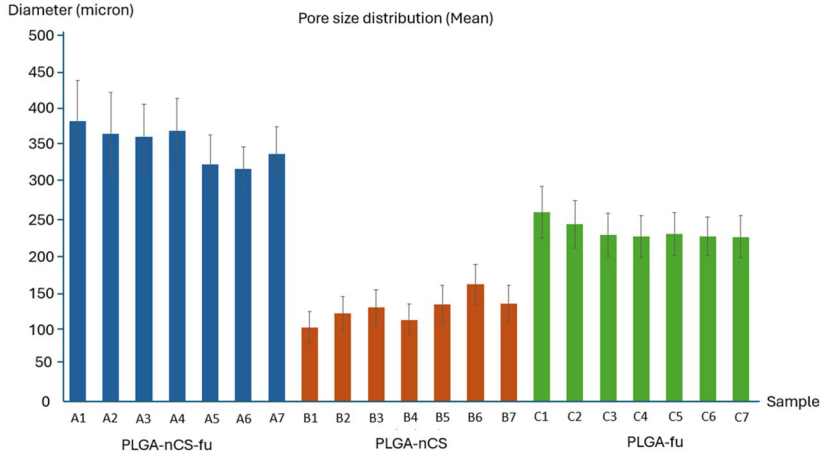

Figure 4. The figure shows the mean pore size distribution for three different types of biomaterial composites: PLGA-nCS-fu, PLGA-nCS and PLGA-fu, across different samples (A1–A7, B1–B7 and C1–C7, respectively). The y-axis represents the pore diameter (in microns), while the x-axis indicates the individual samples for each composite type. The bars indicate the average pore size for each sample, with error bars showing the variability or standard deviation in the measurements. All groups passed the normality test (Shapiro–Wilk, $p > 0.05$), and variance homogeneity was confirmed (Levene's test, $p > 0.05$). One-way ANOVA revealed statistically significant differences among the scaffold groups ($p < 0.05$), suggesting that scaffold composition had a significant impact on the measured outcomes.

Table 1. Summary of pore size distribution for the three scaffold compositions: (A) PLGA-nCS-fu, (B) PLGA-nCS and (C) PLGA-fu. The table presents the mean pore size, standard deviation, and minimum–maximum pore size values (in μm) based on microCT measurements ($n = 1400$ data points per material group).

Material	A (PLGA-nCS-fu)	B (PLGA-nCS)	C (PLGA-fu)
Mean pore size (μm)	354.58	129.03	235.80
Standard deviation	44.96	28.03374	35.5673
Minimum–maximum pore size (μm)	320.29–373.49	102.85–162.19	227.91–260.59

Table 2. Comparison of porosity values for different biomaterial samples, including PLGA-nCS-fu, PLGA-nCS and PLGA-fu. The porosity of these samples was determined through 3D reconstruction from micro-CT images and mimic materialize software, providing insight into the internal structure and pore distribution of each composite material.

PLGA-nCS-fu	PLGA-nCS	PLGA-fu
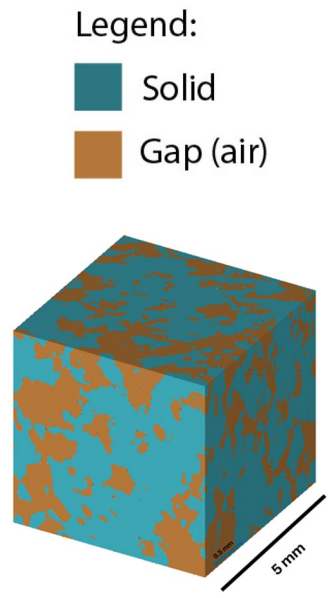	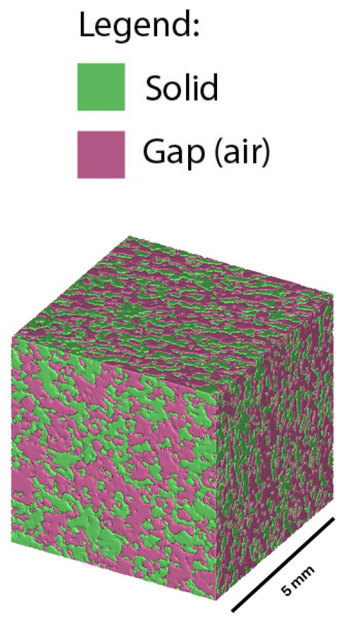	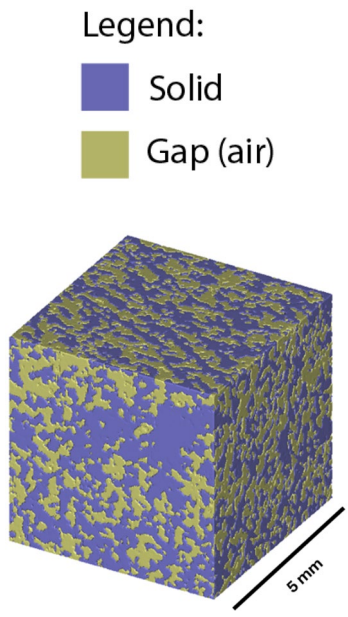
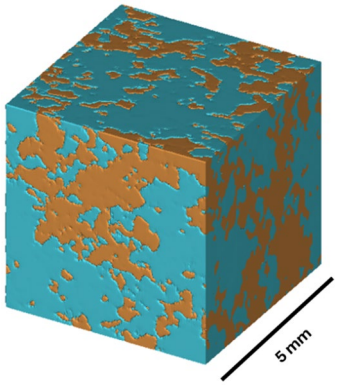 A2: porosity 48%	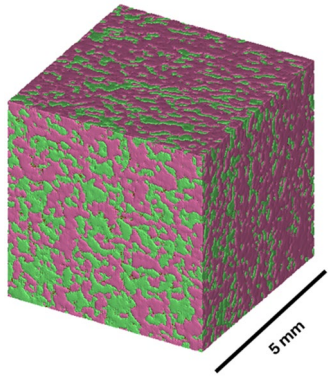 B2: porosity 27%	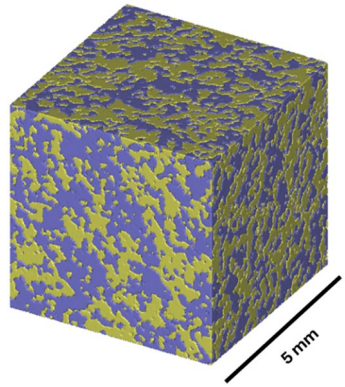 C2: porosity 46%
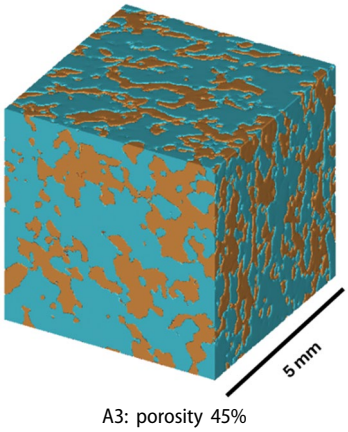 A3: porosity 45%	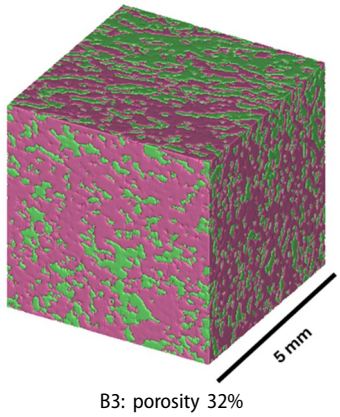 B3: porosity 32%	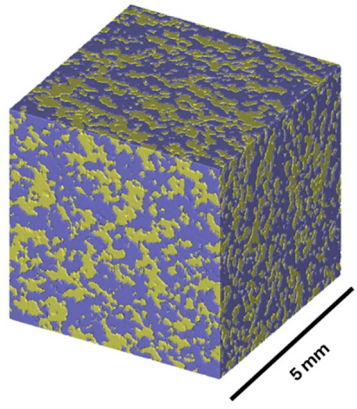 C3: porosity 35%

(*Continued*)

Table 2. Continued.

PLGA-nCS-fu	PLGA-nCS	PLGA-fu
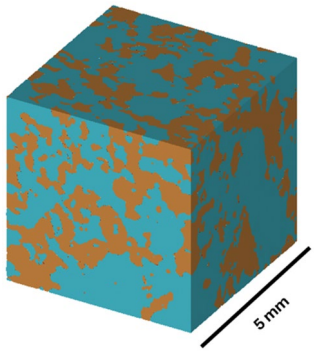 A4: porosity 35%	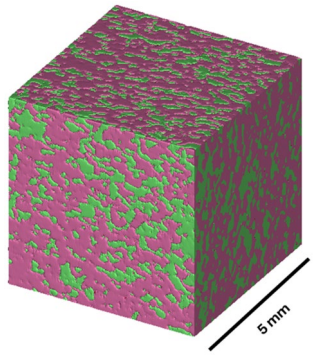 B4: porosity 33%	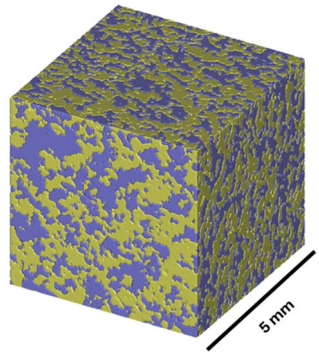 C4: porosity 49%
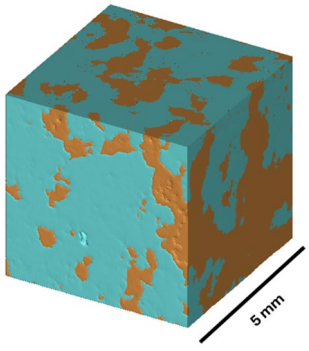 A5: porosity 20%	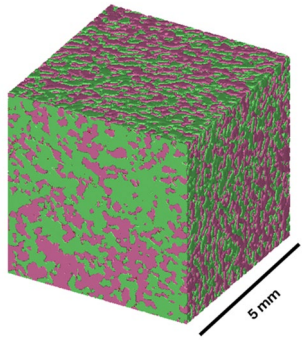 B5: porosity 12%	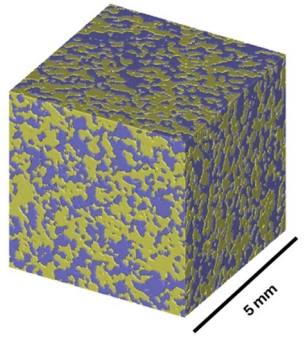 C5: porosity 49%
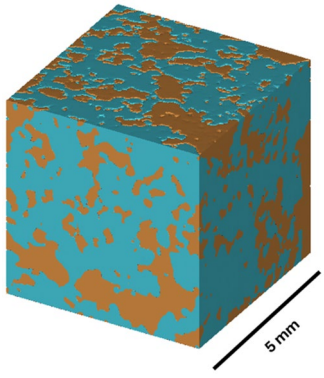 A6: porosity 41%	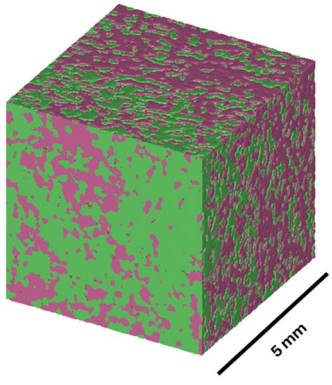 B6: porosity 22%	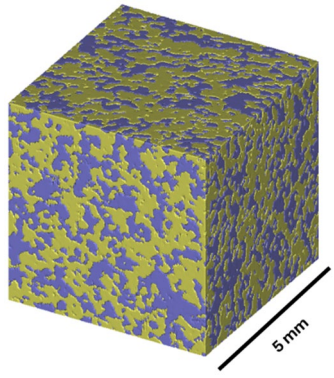 C6: porosity 52%
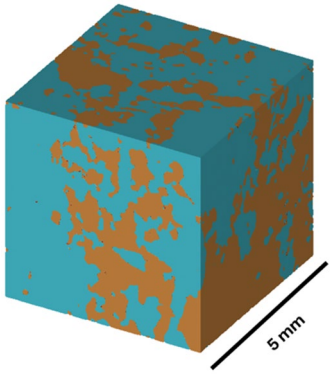 A7: porosity 35%	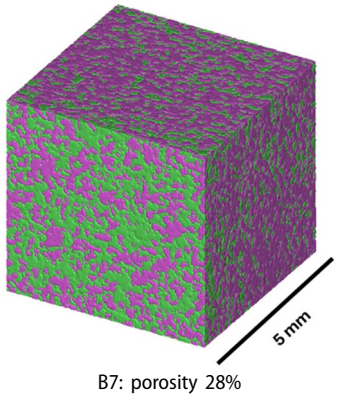 B7: porosity 28%	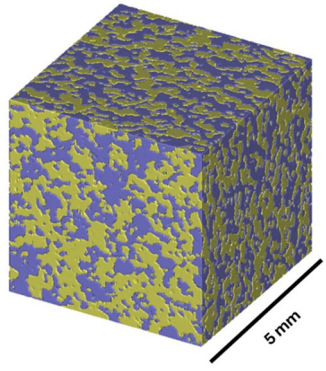 C7: porosity 46%

peaks, reflecting uniform pore sizes and densities. This indicates that fu contributes to better dispersion of the nCS particles, resulting in more controlled and even pore formation. Furthermore, the inclusion of fu affects the overall density distribution within the composite. PLGA-nCS-fu materials have larger pore sizes and a broader pore distribution, which enhances fluid permeability and may improve the material's biological performance, particularly in bone healing applications.

In all datasets, histograms were used to quantify microstructural properties by adjusting the minimum and maximum grey values to align with the specific densities of each material. Through setting different grey scale values, the analysis for each sample was fine-tuned to accurately reflect the distribution of pores and material phases [18,19]. This approach enabled a precise comparison of dense and porous regions between PLGA-nCS and PLGA-nCS-fu materials. In the PLGA-nCS samples, the histogram range was narrower, indicating fewer variations in density and porosity. In contrast, the histograms for PLGA-nCS-fu materials had broader ranges, reflecting greater variability in density and pore size distribution.

These differences are crucial for understanding the mechanical behaviour and biological potential of these composites, as pore size and distribution directly influence tissue in growth rates and the degradation profile of the scaffold [20,21]. The use of histograms was instrumental in highlighting these distinctions, as varying the minimum and maximum values provided a more detailed understanding of porosity and density distribution. PLGA-nCS-fu materials showed a wider distribution of grey values, indicating greater variability in density, likely due to the incorporation of fu, which contributes to a more porous and less dense structure. In contrast, PLGA-nCS materials displayed a relatively narrower distribution, reflecting a more uniform microstructure with less variation in pore size and density.

The lack of gap bubbles in the freeze-dried PLGA-nCS-fu compared to PLGA-nCS is attributed to the presence of fu in the mixture. fu, known for its hydrophilic properties, can effectively absorb and retain water [22]. These characteristics contribute to a more uniform distribution of the solution, resulting in a controlled sublimation process during freeze-drying [23]. fu helps maintain the structural integrity of the material, preventing the formation of large bubbles [24]. Additionally, fu increases the viscosity of the solution prior to freeze-drying [25], which stabilizes the mixture and prevents structural collapse or the formation of gaps caused by rapid gas escape.fu may chemically interact with PLGA and nCS, potentially modifying the matrix and influencing degradation dynamics. These interactions could result in a denser matrix capable of retaining moisture more effectively, thereby reducing hole formation by facilitating delayed and consistent sublimation. The incorporation of fu also alters the thermal characteristics of the compound, including its freezing point and sublimation heat, impacting the vapour release during freeze-drying and reducing the development of substantial vapour pathways (bubbles). These combined effects produce a freeze-dried product with no visible gaps or bubbles, characterized by a more uniform and dense structure compared to PLGA-nCS without fu.

Moreover, dichloromethane (DCM) plays a key role as a volatile organic compound that evaporates at room temperature and during freeze-drying, leading to the formation of gas bubbles as it transitions from liquid to gas [26,27]. fu increases the viscosity of the mixture and creates a more stable matrix [28,29], inhibiting the formation of channels through which DCM can escape. This results in a smoother, more uniform structure without visible gaps. The interaction between fu, PLGA and nCS alters the evaporation dynamics of DCM, effectively trapping the solvent within the matrix and modulating its release rate during the freeze-drying process.

Pore geometry is a crucial factor influencing scaffold performance in inducing bone regeneration [30,31]. Proper pore size enables osteoblasts and mesenchymal stem cells (MSCs) to infiltrate and grow within the scaffold. An optimal pore size (100–500 µm) is essential for facilitating cell migration and proliferation, which promotes tissue formation. Interconnected pores further enhance scaffold functionality by allowing the diffusion of nutrients, oxygen and growth factors necessary for cell survival and tissue growth [30,32]. Additionally, interconnected pores facilitate the removal of waste products, maintaining a healthy environment for cells within the scaffold [33,34].

A scaffold with appropriate pore geometry also supports blood vessel formation (angiogenesis) within the scaffold [35,36]. Blood vessels are vital for long-term tissue survival, ensuring a steady supply of nutrients and oxygen to newly formed bone tissue [30,37]. Moreover, the shape and size of pores impact the scaffold's mechanical strength and stiffness, which must be compatible with the surrounding bone tissue [21,38]. Pore geometry also helps balance the scaffold's strength with its degradation rate, allowing it to support bone formation without collapsing [6,30].

Proper pore geometry promotes osteoconductivity, facilitating the natural growth of new bone along the scaffold's surfaces [39,40]. A well-designed pore geometry serves as a framework that guides bone tissue

growth into the scaffold, supporting integration with native bone [41,42]. This integration is critical for achieving functional and structural compatibility with the host tissue, making pore geometry a key consideration in scaffold design for bone tissue engineering.

The pore size of bone scaffolds is critical for facilitating cell infiltration, nutrient exchange, vascularization and new bone formation [36,43]. The optimal pore size for bone scaffolds typically ranges from 300 to 500 µm [40]. This range has been shown to promote osteoblast adhesion and proliferation, MSC differentiation, and vascularization. Smaller pores (100–200 µm) are more suitable for initial cell attachment, while larger pores (300–500 µm) are better suited for vascularization and bone formation. Studies have identified the 300–400 µm range as optimal, as it effectively balances osteoconductivity and mechanical strength [44].

Influence porosity in mechanical strength

The porosity of scaffolds plays a crucial role in determining their mechanical properties, permeability and biological performance, particularly in tissue engineering applications [45]. Analyses focus on overall porosity shape, pore distribution, porosity levels and the biological implications of these structures (Figure 1). The PLGA-nCS-fu material exhibits a denser matrix with fewer and smaller pores, as evidenced by its lower porosity percentages, ranging from 29.6% to 41.4%. The inclusion of fu enhances the compactness of the polymer structure, reducing pore size and affecting pore connectivity [46]. This compactness may be advantageous in applications requiring controlled release of bioactive molecules or prioritizing mechanical strength. In contrast, the PLGA-nCS sample, with porosity levels between 58.3% and 68.9%, demonstrates a more open structure with larger and better-connected pores [47]. This structural openness suggests that PLGA-nCS may facilitate superior transport properties, including improved nutrient and oxygen diffusion, which are critical for supporting cell proliferation within the scaffold.

In terms of pore distribution, PLGA-nCS-fu and PLGA-fu materials exhibit a more uniform but less distributed pore structure throughout the matrix. This uniformity might reflect the influence of fu during fabrication, potentially inhibiting the formation of larger or more interconnected pores [24]. On the other hand, PLGA-nCS material exhibits a wider range of pore sizes and a higher degree of interconnectivity. This structural openness may provide better mechanical flexibility, advantageous in dynamic biological environments. The porosity level directly affects the scaffold's ability to support cell attachment and proliferation [48]. Although PLGA-nCS-fu has lower porosity than PLGA-nCS, previous *in vitro* results show that PLGA-nCS-fu has a greater biological effect on MSCs [15]. This may be due to the higher porosity of PLGA-nCS arising from defects during the freeze-drying process, while the pore size of PLGA-nCS-fu is more consistent throughout the material.

Additionally, the presence of fu, known for its bioactive properties, may compensate for the lower porosity of PLGA-nCS-fu by promoting selective cell adhesion and differentiation [49,50]. This makes PLGA-nCS-fu potentially more suitable for applications requiring targeted therapeutic interventions or controlled biological responses [51]. In contrast, the higher porosity and interconnectivity of PLGA-nCS material may contribute to its extensive cell proliferation capabilities. These findings highlight the importance of tailoring scaffold properties to match specific biological and mechanical requirements, demonstrating that material composition significantly impacts scaffold performance in biomedical applications. This comparative analysis highlights the need for further research to explore specific cell-scaffold interactions facilitated by fu in the PLGA matrix and to optimize the balance between porosity and bioactivity for various therapeutic applications.

Analysing pore size diameter using Mimics Materialize ensures that bone scaffolds meet biological, mechanical, and clinical requirements, facilitating effective bone regeneration and long-term success in implantation [52,53]. Mimics enables precise measurement of pore size, ensuring that the scaffold meets these biological criteria. A pore size of 300–400 µm is considered ideal, as it allows for the infiltration of osteoblasts, blood vessels and nutrients, thereby promoting new bone formation and vascularization. Studies, such as those by Mikael, suggest that pore sizes around 200–400 µm provide a favourable environment for osteogenesis, encouraging the differentiation of MSC into osteoblasts, which are crucial for bone formation [54,55].

Simon et al. reported that scaffolds with random pore sizes supported continuous bone ingrowth from the outer periphery, while solid walls led to discontinuous ingrowth characterized by bone islands throughout the scaffold. In contrast, scaffolds with uniformly sized pores and porous walls facilitated both continuous and discontinuous bone ingrowth, enabling bone formation not only from the margins but also throughout the entire defect area. This demonstrates that a well-designed porous structure enhances osteogenesis during both *in vitro* and *in vivo* processes [39]. These findings emphasize the importance of tailoring

scaffold pore geometry to optimize bone regeneration outcomes.

Bone scaffolds must facilitate the flow of nutrients, oxygen, and waste products to ensure cell viability and tissue regeneration [33,34]. Optimal pore sizes play a crucial role in enabling this exchange, promoting effective bone healing. Mimics Materialize provides precise 3D analysis, allowing researchers to evaluate whether the pore structure supports this essential exchange [56]. Scaffolds with average pore sizes between 160 and 500 µm are sufficient to promote new bone formation [57]. However, excessively large pore sizes (greater than 400 µm) can compromise the scaffold's mechanical strength, which is critical for load-bearing applications [58].

The optimal pore size range for supporting cell proliferation in regenerative applications has been extensively studied. For load-bearing bone grafts, a pore size range of 50–500 µm is recommended [59]. Larger pores (greater than 300 µm) have been shown to facilitate vascularization, while smaller pores (less than 150 µm) allow cells to pass directly across them, and pores larger than 200 µm provide space for cell occupancy [39,60,61]. A balance between porosity, pore size, and mechanical stability is a crucial aspect of successful bone implantation [62]. Mimics aids in simulating and analysing these factors, helping researchers optimize the balance between porosity and mechanical strength for improved scaffold design [6,21].

To complement the microCT-based analysis of macroporosity and mechanical anisotropy, previously published Brunauer–Emmett–Teller (BET) surface area and pore size distribution data provide critical insights into the scaffold's micro and mesoporous characteristics. Using the BET nitrogen adsorption method, it was observed that PLGA-nCS-fu composites exhibited a relatively lower specific surface area (0.95 m^2/g) compared to PLGA-fu (1.69 m^2/g) and PLGA-nCS (174 m^2/g) [15]. This reduction may have facilitated the earlier release of osteogenic cues, contributing to enhanced gene expression *in vitro*. Furthermore, the pore size of PLGA-nCS-fu was heterogeneous, ranging between 2 and 10 nm, aligning with literature reports that nanopores in the 2–10 nm range can induce osteogenic differentiation of stromal cells. These findings previously reported by Shaz et al. (2024), also revealed that compositional variations significantly influence scaffold surface architecture, with all composites exhibiting Type IV isotherms with hysteresis loops indicative of mesoporosity. When considered alongside the current microCT and FEA results, these data reinforce the importance of multi-scale porosity and anisotropy in optimizing scaffold performance for bone tissue engineering.

Discussion

The purpose of this study was to evaluate the isotropic and anisotropic mechanical properties of three PLGA-based composite materials (PLGA-nCS-fu, PLGA-nCS and PLGA-fu) to assess their potential for bone tissue engineering applications. The p value for sample A is 0.17 (Figure 4), indicating that the population means are not significantly different ($p > 0.05$) across different directions. This suggests that the mechanical properties, such as stiffness or elasticity, do not vary significantly with direction, implying isotropic behaviour. The mechanical behaviour of bone graft materials, whether isotropic or anisotropic, is critical for their suitability in various biomedical applications [2,12]. Isotropic materials, like PLGA-nCS-fu, exhibit consistent properties in all directions, simplifying their use in applications that require uniform mechanical performance. Thus, a p value greater than 0.05 for directional differences in ANSYS analysis confirms that the PLGA-nCS-fu material behaves isotropically for the analysed properties.

In contrast, samples B (PLGA-nCS) and C (PLGA-fu) (Figure 4) show significant differences in mechanical properties across different directions ($p < 0.05$), indicating anisotropic behaviour. Anisotropy in materials means that their properties, such as stiffness or elasticity, vary depending on the direction of measurement. This directional dependency is particularly relevant for bone tissue engineering, as natural bone is inherently anisotropic. Anisotropic scaffolds, such as PLGA-nCS and PLGA-fu, have the potential to mimic the natural variability of bone, supporting enhanced cell adhesion, proliferation and tissue formation [6,63]. Understanding these anisotropic properties is critical for optimizing the design and application of PLGA-based composites for bone regeneration. Through identifying how nCS or fu enhances directional properties, researchers can determine which composite is better suited for specific structural or load-bearing applications in bone repair [5,64].

The significant p values (<0.05) for samples B and C confirm that the observed differences in mechanical properties are inherent to the composition and structure of each material, rather than random variation. This anisotropic behaviour may result from the distinct interactions between PLGA and the additives (nCS and fu), which influence the alignment or distribution of material phases within the composite. These

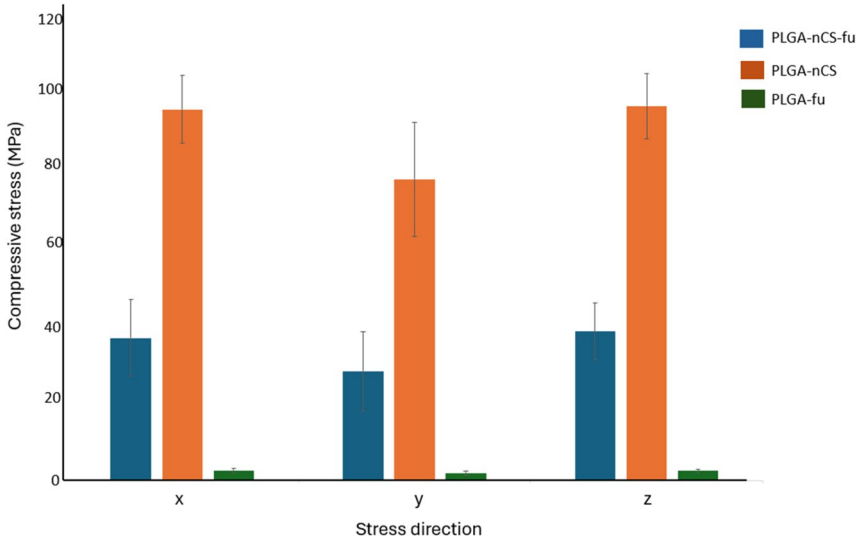

Figure 5. The figure presents the compressive stress values of three different biomaterial composites: PLGA-nCS-fu, PLGA-nCS and PLGA-fu-across three different compression directions: X, Y and Z. Each bar represents the mean stress value for a specific material and direction, with error bars indicating the variability of the data. The compressive stress is given in megapascals (MPa). Sample A (PLGA-nCS-fu): p value = 0.17, $p > 0.05$. This indicates that the differences in stress values for PLGA-nCS-fu are statistically no significant differences (isotropic). Sample B (PLGA-nCS): p value = 0.007, $p < 0.05$. This shows that the differences between the stress values for PLGA-nCS are statistically significant differences (anisotropic). Sample C (PLGA-fu): p value = 0.03, $p < 0.05$. This indicates that the differences in stress values for PLGA-fu are statistically significant differences (anisotropic).

interactions affect mechanical performance under directional forces, explaining the importance of understanding and controlling these properties for optimal biomedical applications.

The observed increase in pore size and heterogeneity in the PLGA-nCS-fu scaffold, as quantified through microCT and confirmed *via* BET analysis, suggests that the inclusion of both nCS and fu modifies the internal microarchitecture in a way that favours osteogenic differentiation [15]. This is consistent with previous findings by Viswanathan et al. and Yin et al., who reported that hierarchical porosity supports stem cell adhesion and nutrient exchange [65,66]. However, our data further indicate that such heterogeneity correlates with anisotropic mechanical responses, particularly along the x- and y-axes, as demonstrated in the FEA simulations. This finding diverges from earlier studies that treated mechanical anisotropy as a limitation rather than a design parameter. Clinically, this implies that tailoring scaffold anisotropy may be essential for load-bearing bone sites where directional stress distribution governs implant performance. Future translational efforts should thus explore the integration of multiscale fabrication techniques, such as 3D bioprinting to control anisotropy while ensuring biological compatibility [67,68]. Moreover, longitudinal *in vivo* models could validate how scaffold architecture dynamically influences bone remodelling, especially under physiological loading conditions [69].

Anisotropic behaviour and mechanical properties

Sample A exhibits similar stress values across all directions, indicating isotropic behaviour based on a statistical analysis p value of 0.05, that shows in Figure 5. This means the mechanical properties are evenly distributed, providing consistent stiffness and strength regardless of the direction of the applied load. In contrast, Samples B and C exhibit significant differences in stress values between different directions, indicating anisotropy that shown in Table 3. This suggests that these materials have a preferred direction for strength and stiffness, akin to natural bone, which is structurally optimized to resist loads in specific directions [70,71].

Among the three materials, the PLGA-nCS composite demonstrated the most pronounced anisotropic behaviour, with higher stiffness and strength observed in preferred loading directions. The addition of both nCS and fu appears to synergistically enhance the structural integrity of PLGA. This combination creates a material with isotropic characteristics, meaning its mechanical properties remain consistent regardless of the direction of loading. Isotropic materials offer consistent mechanical performance in all directions, simplifying the design and application of implants and bone grafts. This uniformity reduces the need for precise alignment during surgery, making these materials easier to use and more adaptable to varying surgical conditions.

Table 3. The FEA results for evaluating the anisotropic mechanical properties of three different composite materials used for bone tissue engineering: PLGA-nCS-fu, PLGA-nCS and PLGA-fu. The analysis assesses medium stress values along the X, Y and Z axes for each sample group, indicating their mechanical response under compression along different orientations.

PLGA-nCS-fu			
Sample	X-axis compression	Y-axis compression	Z-axis compression
A1	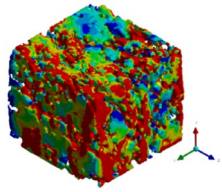 Med stress: 36.9 MPa	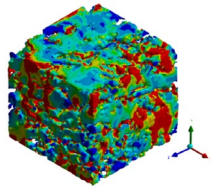 Med stress: 25.2 MPa	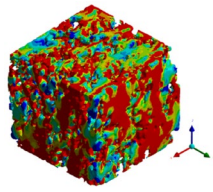 Med stress: 40.0 MPa
A2	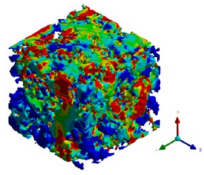 Med stress: 27.6 MPa	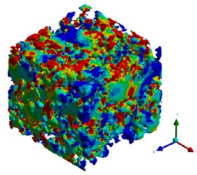 Med stress: 24.3 MPa	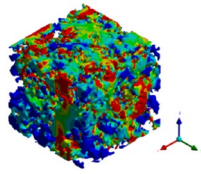 Med stress: 29.5 MPa
A3	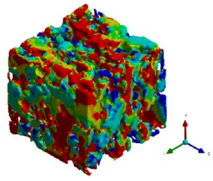 Med stress: 25.4 MPa	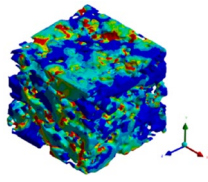 Med stress: 17.6 MPa	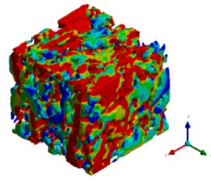 Med stress: 38.9 MPa
A4	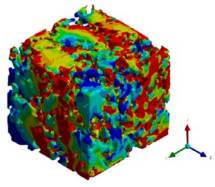 Med stress: 32.1 MPa	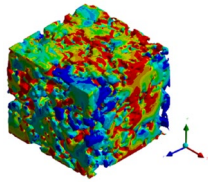 Med stress: 33.7 MPa	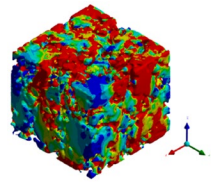 Med stress: 33.9 MPa
A5	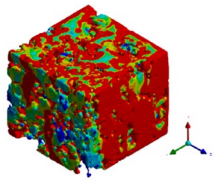 Med stress: 55.8 MPa	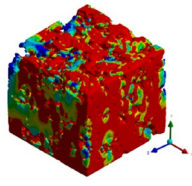 Med stress: 50.8 MPa	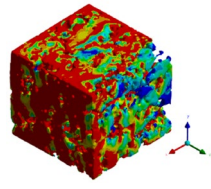 Med stress: 53.8 MPa
A6	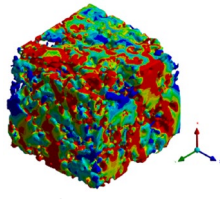 Med stress: 35.6 MPa	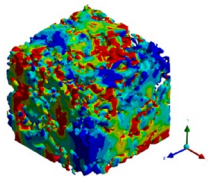 Med stress: 25.0 MPa	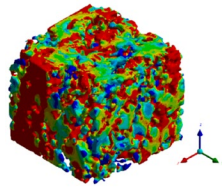 Med stress: 40.5 MPa
A7	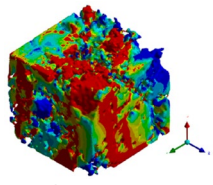 Med stress: 25.4 MPa	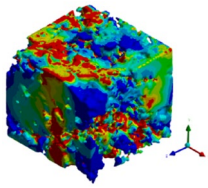 Med stress: 21.5 MPa	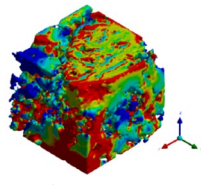 Med stress: 33.6 MPa

(*Continued*)

Table 3. Continued.

PLGA-nCS-fu			
Sample	X-axis compression	Y-axis compression	Z-axis compression
	PLGA-nCS		
B1	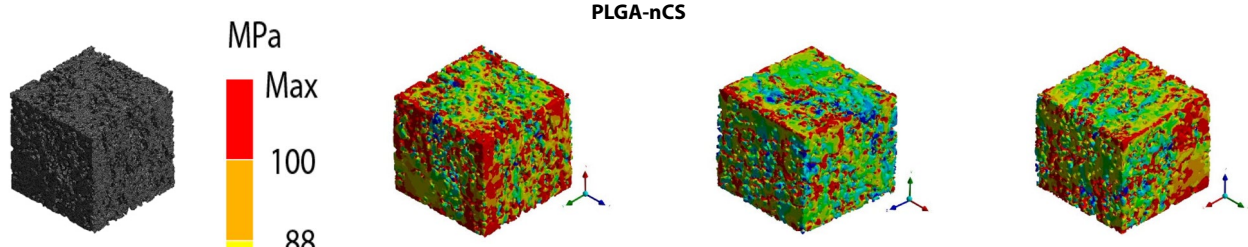 Med stress: 96.5 MPa	Med stress: 83.2 MPa	Med stress: 96.7 MPa
B2	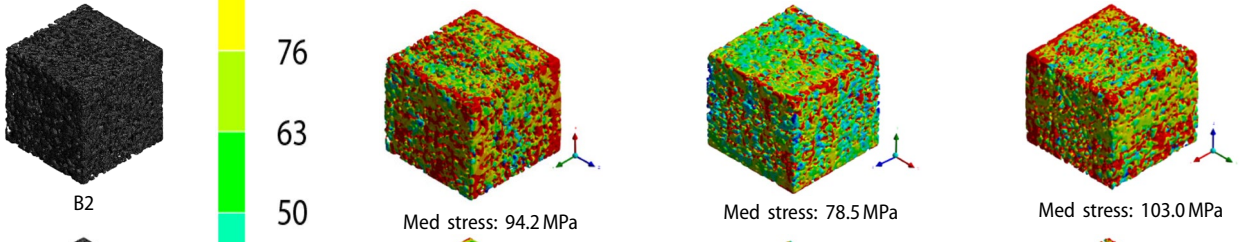 Med stress: 94.2 MPa	Med stress: 78.5 MPa	Med stress: 103.0 MPa
B3	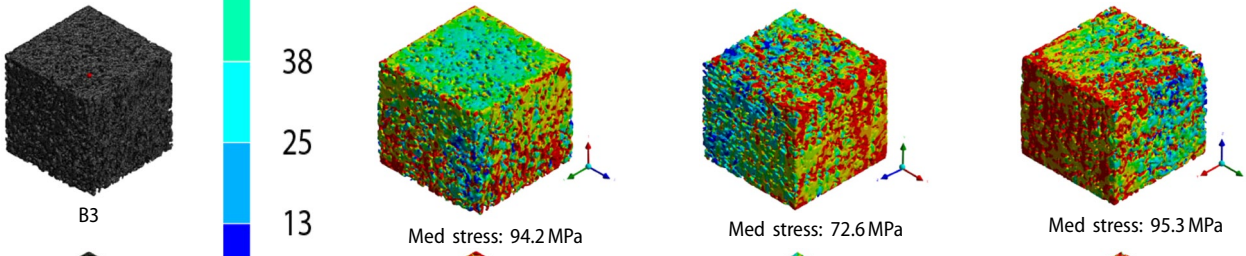 Med stress: 94.2 MPa	Med stress: 72.6 MPa	Med stress: 95.3 MPa
B4	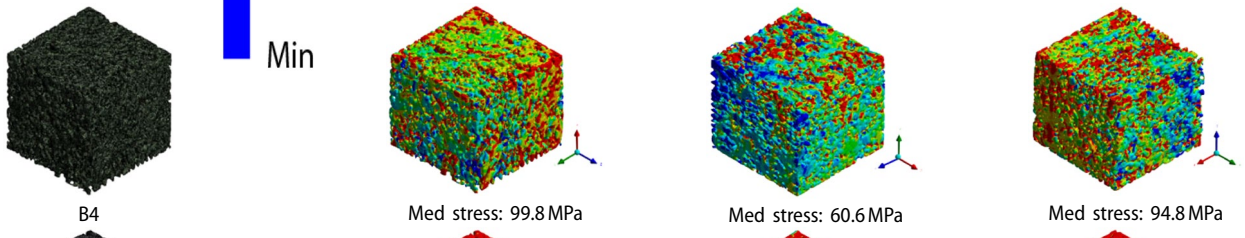 Med stress: 99.8 MPa	Med stress: 60.6 MPa	Med stress: 94.8 MPa
B5	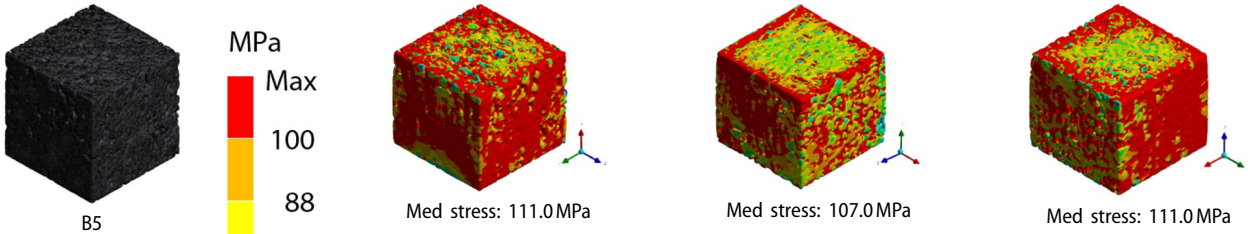 Med stress: 111.0 MPa	Med stress: 107.0 MPa	Med stress: 111.0 MPa
B6	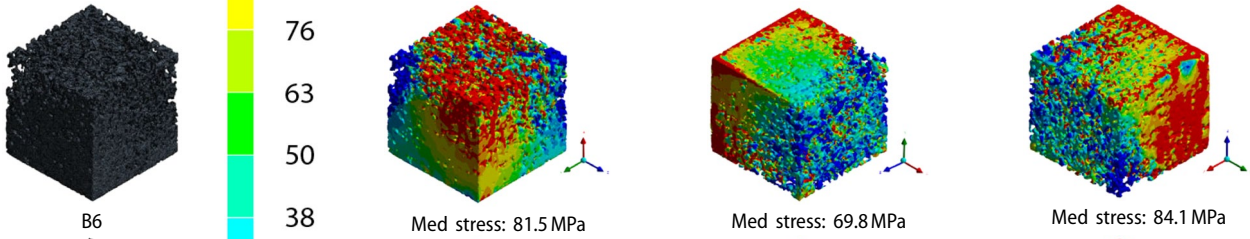 Med stress: 81.5 MPa	Med stress: 69.8 MPa	Med stress: 84.1 MPa
B7	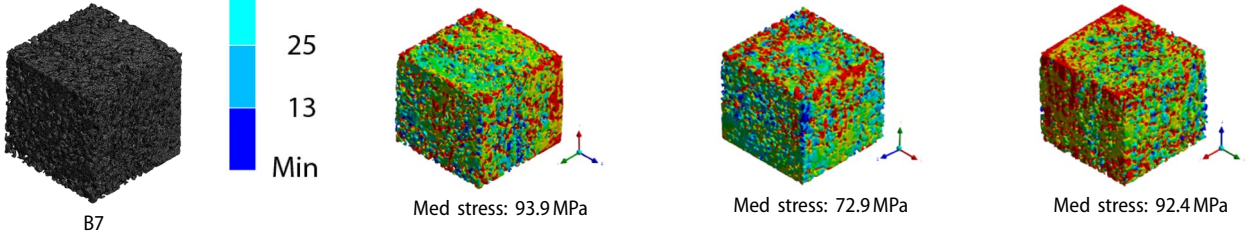 Med stress: 93.9 MPa	Med stress: 72.9 MPa	Med stress: 92.4 MPa

(*Continued*)

Table 3. Continued.

PLGA-nCS-fu			
Sample	X-axis compression	Y-axis compression	Z-axis compression
PLGA-fu			
Sample	X-axis compression	Y-axis compression	Z-axis compression
C1	Med stress: 2.8 MPa	Med stress: 2.2 MPa	Med stress: 2.8 MPa
C2	Med stress: 2.1 MPa	Med stress: 1.6 MPa	Med stress: 2.1 MPa
C3	Med stress: 3.1 MPa	Med stress: 2.4 MPa	Med stress: 3.1 MPa
C4	Med stress: 2.1 MPa	Med stress: 1.6 MPa	Med stress: 2.3 MPa
Sample	X-axis compression	Y-axis compression	Z-axis compression
C5	Med stress: 3.2 MPa	Med stress: 2.7 MPa	Med stress: 3.2 MPa
C6	Med stress: 2.4 MPa	Med stress: 1.6 MPa	Med stress: 2.2 MPa
C7	Med stress: 2.5 MPa	Med stress: 1.4 MPa	Med stress: 2.2 MPa

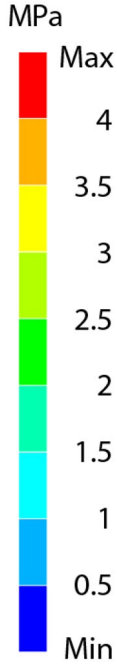

This finding aligns with previous studies suggesting that the inclusion of both organic and inorganic additives can significantly improve PLGA's mechanical properties [9,72]. nCS provides structural reinforcement, enhancing stiffness and strength [73], while fu contributes to bioactivity and mechanical support, resulting in a material with balanced properties suited for bone tissue engineering [23,74].

The PLGA-nCS and PLGA-fu composites exhibit directional dependency in their mechanical properties, akin to natural bone, which demonstrates varying strengths along different axes. This characteristic makes these composites well-suited for load-bearing applications or regions of the body subjected to complex and directional forces. With mimicking the natural anisotropic behaviour of bone, these composites offer improved integration, efficient load transfer and enhanced long-term success in high-stress regions, such as long bones or joints [75,76]. The reinforcement properties of nCS contribute to the additional strength of PLGA-nCS, albeit with reduced flexibility. This performance suggests that PLGA-nCS is a promising candidate for bone tissue engineering in scenarios where moderate directional strength is sufficient.

In contrast, the PLGA-fu composite exhibited the least anisotropic behaviour among the three materials. While Fu enhances the bioactivity of the composite from previous report, it appears to contribute less significantly to directional mechanical strength compared to nCS [15,77]. However, its anti-inflammatory and osteogenic properties make PLGA-fu an appealing option for applications where bioactivity and cell interaction are prioritized over high mechanical strength. This positions PLGA-fu as a versatile material for scenarios where biological responses take precedence, such as in scaffolds designed for tissue regeneration or non-load-bearing applications.

Implications for bone tissue engineering

The clinical application of bone graft substitutes necessitates a careful balance between mechanical integrity and biological efficacy. The results indicate that PLGA-nCS (Sample B) is best suited for high-load-bearing sites where mechanical robustness is paramount. PLGA-nCS-fu (Sample A) offers a promising option for scenarios requiring both structural integrity and enhanced biological activity, such as sites demanding moderate mechanical strength combined with fu's healing-promoting properties. Meanwhile, PLGA-fu (Sample C) may be more appropriate for non-load-bearing applications, leveraging its biological benefits, such as promoting cell attachment and anti-inflammatory effects, rather than relying on mechanical strength.

This study highlights PLGA-nCS as a promising material for bone scaffolds, particularly due to its anisotropic properties, which more closely replicate the load-bearing characteristics of natural bone. Its superior mechanical performance in specific loading directions meets the requirements for bone tissue engineering, where scaffold materials must support varied loads without structural failure. While PLGA-nCS-fu and PLGA-fu may not exhibit the same level of anisotropy as PLGA-nCS, they each offer distinct advantages. PLGA-nCS-fu may be ideal for scaffolds in non-load-bearing bone regions due to its moderate strength, whereas PLGA-fu is well-suited for applications prioritizing bioactivity, such as promoting early-stage bone regeneration and reducing inflammation. These findings show the need for material selection tailored to the specific demands of the intended clinical application.

This study primarily aimed to explore the comparative mechanical behaviour and anisotropic performance of PLGA-based biocomposites (PLGA-nCS, PLGA-fu and PLGA-nCS-fu) using FEA as a predictive tool. Rather than absolute quantitative validation, the focus was on identifying relative trends and structural differences attributable to material composition. To ensure computational efficiency without compromising result accuracy, a mesh convergence procedure was conducted. Tetrahedral (Tet-4) elements were used, yielding final models with 850,000–1,000,000 elements [78]. This corresponded to an element size approximately 1.4% of the total model width, a ratio in accordance with previous FEA guidelines for biological materials. Additional mesh refinement beyond this threshold produced <2% variation in total deformation and von Mises stress, while significantly increasing computational load. Thus, this density was considered optimal for comparative modelling.

All models were constructed using consistent mesh density, boundary conditions and geometric dimensions to eliminate confounding factors and isolate the impact of scaffold composition on mechanical responses. However, it is acknowledged that material parameters, such as Young's modulus and Poisson's ratio were derived from literature values rather than experimental measurements, a limitation that may affect the absolute accuracy of the simulation outputs. Moreover, while a mesh refinement check was performed, a full mesh sensitivity or parametric analysis was not conducted due to hardware limitations. These omissions are transparently noted as limitations of the current modelling strategy.

Future work will address these constraints by integrating mechanical testing data from fabricated scaffolds to calibrate the material models, conducting comprehensive mesh convergence analyses and exploring dynamic and non-linear boundary conditions to more accurately replicate physiological environments. Despite these limitations, the comparative findings from this FEA framework remain robust and meaningful, as the identical meshing and simulation parameters across all groups allow confident interpretation of the observed anisotropy and mechanical trends as being due to compositional differences, not numerical artefacts.

Limitations and challenges

FEA provides a powerful tool for exploring the mechanical response of biomaterial scaffolds under various loading conditions; however, it is inherently constrained by a set of idealized assumptions. This study applied static, uniform loading and assumed homogeneous material properties, which may not fully replicate the complex and dynamic environment of the human body. Furthermore, the simulations do not account for time-dependent factors, such as biodegradation [79], tissue remodelling [80] or biofluid interactions [81], which are critical for clinical relevance.

Although compression testing of the fabricated scaffolds has been performed and reported in a related study [15], biological validation (*in vivo* cellular response [82] and tissue integration [86]) remains to be fully addressed in future phases of this research. Hence, the conclusions drawn from the FEA are predictive in nature and should be interpreted as part of a broader scaffold evaluation framework, not as definitive clinical outcomes. Future work will incorporate long-term degradation modelling [83], dynamic physiological loading [84] and experimental validation, including animal models [85], to assess how anisotropy and material composition influence scaffold integration and functional performance over time.

Conclusion and future directions

FEA provided valuable insights into the mechanical performance of PLGA-based composites with various additives. The inclusion of nCS significantly enhanced compressive strength, positioning PLGA-nCS as a strong candidate for orthopaedic applications requiring high mechanical performance. PLGA-nCS-Fu strikes a balance between mechanical strength and biological benefits, while PLGA-fu is better suited for applications that prioritize biological functionality over mechanical integrity. A key challenge in developing ideal bone grafts lies in replicating the anisotropic nature of natural bone, which exhibits varying mechanical properties depending on the load direction, such as trabecular bone strength differs along anatomical axes. While isotropic materials offer advantages such as uniform load distribution, simpler design, and reduced weak points, they may not fully match natural bone properties and can be less effective for directional loading. Conversely, anisotropic materials mimic natural bone properties, providing optimized load-bearing capabilities and enhanced stability, but they present challenges such as complex manufacturing, uneven load distribution, and the need for precise alignment during surgery.

Further *in vivo* studies are needed to validate these findings and examine the biological effects of these composites on bone regeneration. Experimental testing is essential to corroborate the FEA results and investigate additional factors such as degradation rates, bioactivity and cell-scaffold interactions. Future research should also focus on optimizing the composition and ratios of PLGA, nCS, and Fu to enhance the anisotropic properties of these composites. Doing so could lead to scaffolds that more closely replicate the mechanical and structural properties of natural bone. *In vivo* investigations will be crucial for confirming these results and refining the materials for clinical applications, paving the way for more effective and versatile bone graft solutions.

Statement of originality

The authors declare that this manuscript is original, has not been published before and is not currently being considered for publication elsewhere. The authors confirm that the manuscript has been read and approved by all named authors and that there are no other persons who satisfied the criteria for authorship but are not listed. The authors further confirm that the order of authors listed in the manuscript has been approved by all of us. The authors understand that the Corresponding Author is the sole contact for the Editorial process. The corresponding author is responsible for communicating with the other authors about progress, submissions of revisions and final approval of proofs.

Additional information

No additional information is available for this article.

Clinical trial number

Not applicable.

Institutional review board statement

Not applicable.

Informed consent statement

Not applicable.

Declaration of AI use

The authors declare the use of generative artificial intelligence (AI) and AI-assisted technologies in the preparation of this manuscript. Specifically, ChatGPT (version GPT-4, OpenAI) was used to improve the readability and language of the article. The AI tool was not used for data analysis, interpretation of results, or drawing scientific conclusions. All content has been reviewed and verified by the authors to ensure accuracy and integrity.

Author contributions

Norshazliza Ab Ghani contributed to the conceptualization, data curation and original drafting of the manuscript. She conducted the micro-CT scanning, 3D reconstruction and pore analysis using Mimics Materialize. Mohammed Rafiq Abdul Kadir co-developed the methodology and performed finite element modelling using ANSYS Workbench, in addition to manuscript review and editing. Sathiya Maran supervised the study, supported funding acquisition and contributed to the manuscript's critical revision. Izdihar Kamal provided formal analysis, supervised microstructural interpretation and guided the image processing using Mimics. Muhammad Khalis Abdul Karim conducted statistical analysis using Excel and OriginPro and assisted in sample preparation. Mohd Hafiz Mohd Zaid supported porosity quantification, mesh generation in ANSYS, and data interpretation. Hanumanth Rao Balaji Raghavendran provided supervision and guidance in biomaterial processing. Muhammad Hanif Ramlee assisted with FEA validation and contributed to manuscript review. Tunku Kamarul Zaman provided supervision in scaffold design and data interpretation. Muhammad Imam Ammarullah managed the project, led integration of Mimics and ANSYS, performed visualization and validation, and contributed to manuscript review and final editing.

Transparency statement

The authors affirm that this manuscript is an honest, accurate, and transparent account of the study being reported; that no important aspects of the study have been omitted; and that any discrepancies from the study as planned (and, if relevant, registered) have been explained.

CRediT authorship contribution statement

Norshazliza Ab Ghani: Conceptualization, Data curation and Writing – original draft. Mohammed Rafiq Abdul Kadir: Conceptualization, Methodology and Writing, review, editing. Sathiya Maran: Funding acquisition, Supervision, and Writing – review & editing. Izdihar Kamal: Formal analysis, Resources, and Supervision. Muhammad Khalis Abdul Karim: Investigation, Resources, and Supervision. Mohd Hafiz Mohd Zaid: Methodology, Resources, and Supervision. Hanumanth Rao Balaji Raghavendran: Resources and Supervision. Muhammad Hanif Ramlee: Resources, Supervision, and Writing – review & editing. Tunku Kamarul Zaman: Conceptualization, Data curation and Supervision. Muhammad Imam Ammarullah: Project administration, Software, Validation, Visualization, and Writing – review & editing.

Disclosure statement

The authors declare that they have no known competing financial interests or personal relationships that could have appeared to influence the work reported in this article.

Funding

This work was supported by Monash University Research Grant (ECR-000002), Universitas Sriwijaya Indonesia (grant no.: 1U051) and Ministry of Science, Technology and Innovation (MOSTI) of Malaysia (grant no.: 4S151 and TDF12221651).

ORCID

Norshazliza Ab Ghani http://orcid.org/0009-0009-9093-0749
Mohammed Rafiq Abdul Kadir http://orcid.org/0000-0002-4762-5839
Sathiya Maran http://orcid.org/0000-0001-5617-901X
Izdihar Kamal http://orcid.org/0009-0005-7800-7629
Muhammad Khalis Abdul Karim http://orcid.org/0000-0002-5357-4193
Mohd Hafiz Mohd Zaid http://orcid.org/0000-0001-6734-800X
Hanumanth Rao Balaji Raghavendran http://orcid.org/0000-0001-9374-7223
Muhammad Hanif Ramlee http://orcid.org/0000-0003-2705-8379
Tunku Kamarul Zaman http://orcid.org/0000-0002-6028-1313
Muhammad Imam Ammarullah http://orcid.org/0000-0002-8845-7202

Data availability statement

The necessary data used in the manuscript are already present in the manuscript.

References

[1] Koushik TM, Miller CM, Antunes E. Bone tissue engineering scaffolds: function of multi-material hierarchically structured scaffolds. Adv Healthc Mater. 2023;12(9):e2202766. doi: 10.1002/adhm.202202766.
[2] Liao SH, Tong RF, Dong JX. Anisotropic finite element modeling for patient-specific mandible. Comput Methods Programs Biomed. 2007;88(3):197–209. doi: 10.1016/j.cmpb.2007.09.009.

[3] Chen J, Liu X, Tian Y, et al. 3D-Printed anisotropic polymer materials for functional applications. Adv Mater. 2022;34(5):2102877. doi: 10.1002/adma.202102877.
[4] Kang J, Dong E, Li D, et al. Anisotropy characteristics of microstructures for bone substitutes and porous implants with application of additive manufacturing in orthopaedic. Mater Design. 2020;191:108608. doi: 10.1016/j.matdes.2020.108608.
[5] Evans S, Gregson P. Composite technology in load-bearing orthopaedic implants. Biomaterials. 1998;19(15):1329–1342. doi: 10.1016/s0142-9612(97)00217-2.
[6] Wu S, Liu X, Yeung KWK, et al. Biomimetic porous scaffolds for bone tissue engineering. Mater Sci Eng Rep. 2014;80:1–36. doi: 10.1016/j.mser.2014.04.001.
[7] Zhao D, Zhu T, Li J, et al. Poly(lactic-co-glycolic acid)-based composite bone-substitute materials. Bioact Mater. 2021;6(2):346–360. doi: 10.1016/j.bioactmat.2020.08.016.
[8] Xing J, Liu N, Xu N, et al. Engineering complex anisotropic scaffolds beyond simply uniaxial alignment for tissue engineering. Adv Funct Materials. 2022;32(15):2110676. doi: 10.1002/adfm.202110676.
[9] Liu T, Li Z, Zhao L, et al. Customized design 3D printed PLGA/calcium sulfate scaffold enhances mechanical and biological properties for bone regeneration. Front Bioeng Biotechnol. 2022;10:874931. doi: 10.3389/fbioe.2022.874931.
[10] Fernandes G, Abhyankar V, O'Dell JM. Calcium sulfate as a scaffold for bone tissue engineering: a descriptive review. JDODT. 2021;9(1):1–22. doi: 10.15226/jdodt.2021.001124.
[11] Ahmad T, Eapen MS, Ishaq M, et al. Anti-inflammatory activity of fucoidan extracts in vitro. Mar Drugs. 2021;19(12):702. doi: 10.3390/md19120702.
[12] Kazembakhshi S, Luo Y. Constructing anisotropic finite element model of bone from computed tomography (CT). Biomed Mater Eng. 2014;24(6):2619–2626. doi: 10.3233/BME-141078.
[13] Alemayehu D-B, Jeng Y-R. Three-dimensional finite element investigation into effects of implant thread design and loading rate on stress distribution in dental implants and anisotropic bone. Materials. 2021;14(22):6974. doi: 10.3390/ma14226974.
[14] Dhawan U, Williams JA, Windmill JFC, et al. Engineered surfaces that promote capture of latent proteins to facilitate integrin-mediated mechanical activation of growth factors. Adv Mater. 2024;36(23):2310789. doi: 10.1002/adma.202310789.
[15] Shaz N, Maran S, Genasan K, et al. Functionalization of poly (lactic-co-glycolic acid) nano-calcium sulphate and fucoidan 3D scaffold using human bone marrow mesenchymal stromal cells for bone tissue engineering application. Int J Biol Macromol. 2024;256(Pt 1):128059. doi: 10.1016/j.ijbiomac.2023.128059.
[16] Wei Z, Ou Y, Wang J, et al. Structure-digestibility relationships in the effect of fucoidan on A-and B-wheat starch. Int J Biol Macromol. 2022;215:235–242. doi: 10.1016/j.ijbiomac.2022.06.063.
[17] Mikušová V, Mikuš P. Advances in chitosan-based nanoparticles for drug delivery. Int J Mol Sci. 2021;22(17):9652. doi: 10.3390/ijms22179652.
[18] Palacio-Mancheno PE, et al. 3D assessment of cortical bone porosity and tissue mineral density using high-resolution μCT: effects of resolution and threshold method. J Bone Miner Res. 2014;29(1):142–150. doi: 10.1002/jbmr.2012.
[19] Zidek J, Vojtova L, Abdel-Mohsen AM, et al. Accurate micro-computed tomography imaging of pore spaces in collagen-based scaffold. J Mater Sci: mater Med. 2016;27(6):1–18. doi: 10.1007/s10856-016-5717-2.
[20] Jia G, Huang H, Niu J, et al. Exploring the interconnectivity of biomimetic hierarchical porous Mg scaffolds for bone tissue engineering: effects of pore size distribution on mechanical properties, degradation behavior and cell migration ability. J Magnesium Alloys. 2021;9(6):1954–1966. doi: 10.1016/j.jma.2021.02.001.
[21] Sobral JM, Caridade SG, Sousa RA, et al. Three-dimensional plotted scaffolds with controlled pore size gradients: effect of scaffold geometry on mechanical performance and cell seeding efficiency. Acta Biomater. 2011;7(3):1009–1018. doi: 10.1016/j.actbio.2010.11.003.
[22] Jiang Y, Zhao Y, Liu Z, et al. Roles and mechanisms of fucoidan against dermatitis: a review. Int J Biol Macromol. 2024;279(Pt 3):135268. doi: 10.1016/j.ijbiomac.2024.135268.
[23] Devi GVY, et al. Fucoidan-incorporated composite scaffold stimulates osteogenic differentiation of mesenchymal stem cells for bone tissue engineering. Mar Drugs. 2022;20(10):589. doi: 10.3390/md20100589.
[24] Hao Y, Zheng W, Sun Z, et al. Marine polysaccharide-based composite hydrogels containing fucoidan: preparation, physicochemical characterization, and biocompatible evaluation. Int J Biol Macromol. 2021;183:1978–1986. doi: 10.1016/j.ijbiomac.2021.05.190.
[25] Aranaz I, Gutiérrez MC, Ferrer ML, et al. Preparation of chitosan nanocompositeswith a macroporous structure by unidirectional freezing and subsequent freeze-drying. Mar Drugs. 2014;12(11):5619–5642. doi: 10.3390/md12115619.
[26] Fu Z, Cui J, Zhao B, et al. An overview of polyester/hydroxyapatite composites for bone tissue repairing. J Orthop Translat. 2021;28:118–130. doi: 10.1016/j.jot.2021.02.005.
[27] Erdem A, Haghniaz R, Ertas YN, et al. Methods for fabricating oxygen releasing biomaterials. J Drug Target. 2022;30(2):188–199. doi: 10.1080/1061186X.2021.1971235.
[28] Zhang X, Wei Z, Xue C. Physicochemical properties of fucoidan and its applications as building blocks of nutraceutical delivery systems. Crit Rev Food Sci Nutr. 2022;62(32):8935–8953. doi: 10.1080/10408398.2021.1937042.
[29] Pajovich HT, Banerjee IA. Biomineralization of fucoidan-peptide blends and their potential applications in bone tissue regeneration. J Funct Biomater. 2017;8(3):41. doi: 10.3390/jfb8030041.
[30] Abbasi N, Hamlet S, Love RM, et al. Porous scaffolds for bone regeneration. J Sci: adv Mater Devices. 2020;5(1):1–9. doi: 10.1016/j.jsamd.2020.01.007.
[31] Wu R, Li Y, Shen M, et al. Bone tissue regeneration: the role of finely tuned pore architecture of bioactive scaffolds before clinical translation. Bioact Mater. 2021;6(5):1242–1254. doi: 10.1016/j.bioactmat.2020.11.003.
[32] De Witte T-M, Fratila-Apachitei LE, Zadpoor AA, et al. Bone tissue engineering via growth factor delivery:

from scaffolds to complex matrices. Regen Biomater. 2018;5(4):197–211. doi: 10.1093/rb/rby013.
[33] Chocholata P, Kulda V, Babuska V. Fabrication of scaffolds for bone-tissue regeneration. Materials. 2019;12(4):568. doi: 10.3390/ma12040568.
[34] Collins MN, Ren G, Young K, et al. Scaffold fabrication technologies and structure/function properties in bone tissue engineering. Adv Funct Mater. 2021;31(21):2010609. doi: 10.1002/adfm.202010609.
[35] Mehdizadeh H, Sumo S, Bayrak ES, et al. Three-dimensional modeling of angiogenesis in porous biomaterial scaffolds. Biomaterials. 2013;34(12):2875–2887. doi: 10.1016/j.biomaterials.2012.12.047.
[36] Gupte MJ, Swanson WB, Hu J, et al. Pore size directs bone marrow stromal cell fate and tissue regeneration in nanofibrous macroporous scaffolds by mediating vascularization. Acta Biomater. 2018;82:1–11. doi: 10.1016/j.actbio.2018.10.016.
[37] Badhe RV, Bijukumar D, Chejara DR, et al. A composite chitosan-gelatin bi-layered, biomimetic macroporous scaffold for blood vessel tissue engineering. Carbohydr Polym. 2017;157:1215–1225. doi: 10.1016/j.carbpol.2016.09.095.
[38] Gryko A, Prochor P, Sajewicz E. Finite element analysis of the influence of porosity and pore geometry on mechanical properties of orthopaedic scaffolds. J Mech Behav Biomed Mater. 2022;132:105275. doi: 10.1016/j.jmbbm.2022.105275.
[39] Karageorgiou V, Kaplan D. Porosity of 3D biomaterial scaffolds and osteogenesis. Biomaterials. 2005;26(27):5474–5491. doi: 10.1016/j.biomaterials.2005.02.002.
[40] Wu Y, Liu P, Feng C, et al. 3D printing calcium phosphate ceramics with high osteoinductivity through pore architecture optimization. Acta Biomater. 2024;185:111–125. doi: 10.1016/j.actbio.2024.07.008.
[41] McIntosh L, Cordell J, Johnson AW. Impact of bone geometry on effective properties of bone scaffolds. Acta Biomater. 2009;5(2):680–692. doi: 10.1016/j.actbio.2008.09.010.
[42] Pivonka P, Buenzli PR, Scheiner S, et al. The influence of bone surface availability in bone remodelling—a mathematical model including coupled geometrical and biomechanical regulations of bone cells. Eng Struct. 2013;47:134–147. doi: 10.1016/j.engstruct.2012.09.006.
[43] Liu Y, Yang S, Cao L, et al. Facilitated vascularization and enhanced bone regeneration by manipulation hierarchical pore structure of scaffolds. Mater Sci Eng C Mater Biol Appl. 2020;110:110622. doi: 10.1016/j.msec.2019.110622.
[44] Murphy CM, Haugh MG, O'brien FJ. The effect of mean pore size on cell attachment, proliferation and migration in collagen–glycosaminoglycan scaffolds for bone tissue engineering. Biomaterials. 2010;31(3):461–466. doi: 10.1016/j.biomaterials.2009.09.063.
[45] Foroughi AH, Razavi MJ. Multi-objective shape optimization of bone scaffolds: enhancement of mechanical properties and permeability. Acta Biomater. 2022;146:317–340. doi: 10.1016/j.actbio.2022.04.051.
[46] Lu Y, Cheng L, Yang Z, et al. Relationship between the morphological, mechanical and permeability properties of porous bone scaffolds and the underlying microstructure. PLoS One. 2020;15(9):e0238471. doi: 10.1371/journal.pone.0238471.
[47] Jodati H, Yılmaz B, Evis Z. A review of bioceramic porous scaffolds for hard tissue applications: effects of structural features. Ceram Int. 2020;46(10):15725–15739. doi: 10.1016/j.ceramint.2020.03.192.
[48] Bružauskaitė I, Bironaitė D, Bagdonas E, et al. Scaffolds and cells for tissue regeneration: different scaffold pore sizes—different cell effects. Cytotechnology. 2016;68(3):355–369. doi: 10.1007/s10616-015-9895-4.
[49] Kim BS, Kang H-J, Park J-Y, et al. Fucoidan promotes osteoblast differentiation via JNK-and ERK-dependent BMP2–Smad 1/5/8 signaling in human mesenchymal stem cells. Exp Mol Med. 2015;47(1):e128-e128–e128. doi: 10.1038/emm.2014.95.
[50] Wang F, Xiao Y, Neupane S, et al. Influence of fucoidan extracts from different fucus species on adult stem cells and molecular mediators in in vitro models for bone formation and vascularization. Mar Drugs. 2021;19(4):194. doi: 10.3390/md19040194.
[51] Puvaneswary S, Raghavendran HB, Talebian S, et al. Incorporation of Fucoidan in beta-Tricalcium phosphate-Chitosan scaffold prompts the differentiation of human bone marrow stromal cells into osteogenic lineage. Sci Rep. 2016;6(1):24202. doi: 10.1038/srep24202.
[52] Ivanovski S, Breik O, Carluccio D, et al. 3D printing for bone regeneration: challenges and opportunities for achieving predictability. Periodontol 2000. 2023;93(1):358–384. doi: 10.1111/prd.12525.
[53] Yuan L, Ding S, Wen C. Additive manufacturing technology for porous metal implant applications and triple minimal surface structures: a review. Bioact Mater. 2019;4(1):56–70. doi: 10.1016/j.bioactmat.2018.12.003.
[54] Mikael PE. Hybrid matrix design for cartilage-mediated bone tissue engineering. Mansfield (CT): University of Connecticut; 2015.
[55] Bao C, Zhang B, Li Y, et al. In Vivo bone tissue engineering. Tissue engineering: roles, materials, and applications. Hauppauge (NY): Nova Publishers; 2008. p. 191-242.
[56] Ho ST, Hutmacher DW. A comparison of micro CT with other techniques used in the characterization of scaffolds. Biomaterials. 2006;27(8):1362–1376. doi: 10.1016/j.biomaterials.2005.08.035.
[57] Sakthiabirami K, Soundharrajan V, Kang J-H, et al. Three-dimensional zirconia-based scaffolds for load-bearing bone-regeneration applications: prospects and challenges. Materials. 2021;14(12):3207. doi: 10.3390/ma14123207.
[58] Torres-Sanchez C, Al Mushref FRA, Norrito M, et al. The effect of pore size and porosity on mechanical properties and biological response of porous titanium scaffolds. Mater Sci Eng C Mater Biol Appl. 2017;77:219–228. doi: 10.1016/j.msec.2017.03.249.
[59] Tadic D, Beckmann F, Donath T, et al. Comparison of different methods for the preparation of porous bone substitution materials and structural investigations by synchrotron μ-computer tomography. Materialwissenschaft Werkst. 2004;35(4):240–244. doi: 10.1002/mawe.200400730.
[60] de Wild M, Zimmermann S, Rüegg J, et al. Influence of microarchitecture on osteoconduction and mechanics of porous titanium scaffolds generated by selective laser melting. 3D Print Addit Manuf. 2016;3(3):142–151. doi: 10.1089/3dp.2016.0004.

[61] Xue W, Krishna BV, Bandyopadhyay A, et al. Processing and biocompatibility evaluation of laser processed porous titanium. Acta Biomater. 2007;3(6):1007–1018. doi: 10.1016/j.actbio.2007.05.009.
[62] Wang X, Xu S, Zhou S, et al. Topological design and additive manufacturing of porous metals for bone scaffolds and orthopaedic implants: a review. Biomaterials. 2016;83:127–141. doi: 10.1016/j.biomaterials.2016.01.012.
[63] Chen J. Current advances in anisotropic structures for enhanced osteogenesis. Colloids Surf B Biointerfaces. 2023;231:113566. doi: 10.1016/j.colsurfb.2023.113566.
[64] De Santis R, Guarino V, Ambrosio L. Composite biomaterials for bone repair, in Bone repair biomaterials. Sawston: Woodhead Publishing; 2019. p. 273–299.
[65] Viswanathan P, Ondeck MG, Chirasatitsin S, et al. 3D surface topology guides stem cell adhesion and differentiation. Biomaterials. 2015;52:140–147. doi: 10.1016/j.biomaterials.2015.01.034.
[66] Yin S, Wu H, Huang Y, et al. Structurally and mechanically tuned macroporous hydrogels for scalable mesenchymal stem cell–extracellular matrix spheroid production. Proc Natl Acad Sci USA. 2024;121(28):e2404210121. doi: 10.1073/pnas.2404210121.
[67] Murphy SV, De Coppi P, Atala A. Opportunities and challenges of translational 3D bioprinting. Nat Biomed Eng. 2020;4(4):370–380. doi: 10.1038/s41551-019-0471-7.
[68] Heinrich MA, Liu W, Jimenez A, et al. 3D bioprinting: from benches to translational applications. Small. 2019;15(23):e1805510. doi: 10.1002/smll.201805510.
[69] Long SY, Fu YJ, Zhang ZM, et al. Architecture mechanics mediated osteogenic progression in bone regeneration of artificial scaffolds. Sci Adv. 2025;11(29):eadv8804. doi: 10.1126/sciadv.adv8804.
[70] Liu Z, Zhang Z, Ritchie RO. Structural orientation and anisotropy in biological materials: functional designs and mechanics. Adv Funct Mater. 2020;30(10):1908121. doi: 10.1002/adfm.201908121.
[71] Naleway SE, Porter MM, McKittrick J, et al. Structural design elements in biological materials: application to bioinspiration. Adv Mater. 2015;27(37):5455–5476. doi: 10.1002/adma.201502403.
[72] Rocha CV, Gonçalves V, da Silva MC, et al. PLGA-based composites for various biomedical applications. Int J Mol Sci. 2022;23(4):2034. doi: 10.3390/ijms23042034.
[73] Cai Z, Wu Z, Wan Y, et al. Manipulation of the degradation behavior of calcium phosphate and calcium sulfate bone cement system by the addition of micro-nano calcium phosphate. Ceram Int. 2021;47(20):29213–29224. doi: 10.1016/j.ceramint.2021.07.086.
[74] Vk AD, Udduttula A, Jaiswal AK. Unveiling the secrets of marine—derived fucoidan for bone tissue engineering—A review. Front Bioeng Biotechnol. 2023;10:1100164. doi: 10.3389/fbioe.2022.1100164.
[75] Scholz M-S, Blanchfield JP, Bloom LD, et al. The use of composite materials in modern orthopaedic medicine and prosthetic devices: a review. Compos Sci Technol. 2011;71(16):1791–1803. doi: 10.1016/j.compscitech.2011.08.017.
[76] Budharaju H, Suresh S, Sekar MP, et al. Ceramic materials for 3D printing of biomimetic bone scaffolds–Current state-of-the-art & future perspectives. Mater Design. 2023;231:112064. doi: 10.1016/j.matdes.2023.112064.
[77] Wang Y, Zhao Y, Wang X, et al. Fucoidan/collagen composite coating on magnesium alloy for better corrosion resistance and pro-endothelialization potential. Int J Biol Macromol. 2024;255:128044. doi: 10.1016/j.ijbiomac.2023.128044.
[78] Abdul Kadir MR. Finite element model construction. Computational biomechanics of the hip joint. Berlin, Germany: Springer; 2013. p. 19–42.
[79] Wu XS. Synthesis, characterization, biodegradation, and drug delivery application of biodegradable lactic/glycolic acid polymers: part III. Drug delivery application. Artif Cells Blood Subst Biotechnol. 2004;32:575–591. doi: 10.1081/BIO-200039635.
[80] Breisnes HW, Leeming DJ, Karsdal MA, et al. Biomarkers of tissue remodelling are elevated in serum of COVID-19 patients who develop interstitial lung disease - an exploratory biomarker study. BMC Pulm Med. 2024;24(1):331. doi: 10.1186/s12890-024-03144-0.
[81] Basri H, Syahrom A, Saad APM, et al. The effect of degradation time variation on porous magnesium implant bone scaffold. E3S Web Conf. 2018;68:01019. doi: 10.1051/e3sconf/20186801019.
[82] Dornelas J, Dornelas G, Rossi A, et al. The incorporation of zinc into hydroxyapatite and its influence on the cellular response to biomaterials: a systematic review. J Funct Biomater. 2024;15(7):178. doi: 10.3390/jfb15070178.
[83] Allena R, Scerrato D, Bersani A, et al. Simulating bone healing with bio-resorbable scaffolds in a three-dimensional system: insights into graft resorption and integration. Comptes Rendus. Mécanique. 2025;353(G1):479–497. doi: 10.5802/crmeca.291.
[84] Ammarullah MI, Kozin M, Maula MI, et al. A review of enhanced total hip prosthesis design and material bearing combination to accommodate Muslim prayer (Salat) movements: biomechanical, biotribological, and biological perspectives. Tribol. Int. 2025;205:110518. doi: 10.1016/j.triboint.2025.110518.
[85] Baggio AMP, Sillmann YM, Eber P, et al. How does ceramic-based scaffold microarchitecture impact maxillofacial bone regeneration? A systematic review of large animal models. Appl. Sci. 2025;15:6899. doi: 10.3390/app15126899.
[86] Ranjbar FE, Farzad-Mohajeri S, Samani S, et al. Kaempferol-loaded bioactive glass-based scaffold for bone tissue engineering: in vitro and in vivo evaluation. Sci Rep. 2023;13(1):12375. doi: 10.1038/s41598-023-39505-8.